Water Research 307 (2026) 126751

Contents lists available at ScienceDirect

Water Research

journal homepage: www.elsevier.com/locate/watres

Long-term leaching dynamics and ecotoxicity of wastewater from electric vehicle lithium-ion battery fires

Lucie Pokorna-Krayzelova [a,*], Hana Kujalova [a], Lucia Tajnaiova [b], Klara Anna Mocova [b], Martina Martinková [a], Jana Kofronová [b], Radek Vurm [b], Jakub Pilar [b], Krystof Rehak [b], Barbora Stepanova [c], Petra Najmanova [c], Jan Karl [d], Romana Friedrichova [d], Marek Martinec [b], Jan Bindzar [a]

[a] Department of Water Technology & Environmental Engineering, University of Chemistry and Technology in Prague, Technicka 5, 166 28 Prague 6, Czech Republic
[b] Department of Environmental Chemistry, University of Chemistry and Technology in Prague, Technicka 5, 166 28 Prague 6, Czech Republic
[c] Dekonta, a.s., Dřetovice 109, Stehelčeves, 273 42, Czech Republic
[d] Ministry of the Interior, General Directorate of the HZS – Technical Institute of Fire Protection, Písková 42, 143 00 Prague 4, Czech Republic

HIGHLIGHTS

- First study on 112-day leaching dynamics of submerged EV batteries.
- Runoff conductivity (23.1 mS/cm) reaches levels of landfill leachates.
- Lithium (1.54 g/L) and fluoride (218.2 mg/L) exceed limits by orders of magnitude.
- Long-term immersion causes extreme acute toxicity to *Daphnia magna*.
- Non-ignited, venting batteries still release hazardous organic pollutants.

GRAPHICAL ABSTRACT

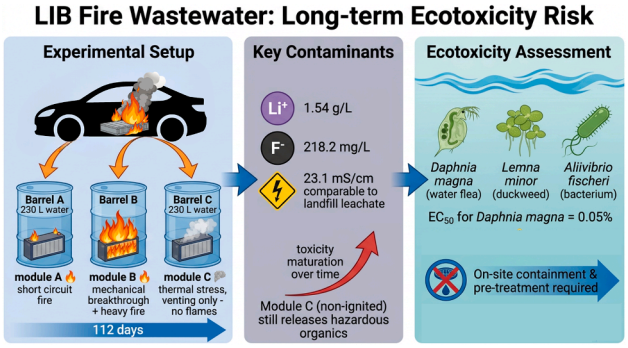

ARTICLE INFO

Keywords:
Ecotoxicity
Electric vehicles
Electromobility
Environmental impact
Fires
Lithium-ion batteries
Wastewater

ABSTRACT

The global adoption of electric vehicles has increased the frequency of lithium-ion battery (LIB) fires, which are typically managed through large-scale water suppression and immersion. While immediate fire behavior is well-documented, the long-term environmental consequences of the resulting wastewater remain poorly understood. This study evaluates the 112-day temporal dynamics of contaminant leaching from nickel-manganese-cobalt (NMC) vehicle batteries following three distinct ignition scenarios: a short circuit, mechanical breakthrough with heavy fire, and thermal stress without visible flames. Physicochemical analysis revealed that the most heavily damaged module exhibited the highest pollutant load in this case study. The module that experienced the most extensive physical damage showed the highest conductivity (23.1 mS/cm), high lithium (1.54 g/L), and elevated fluoride levels (218 mg/L), exceeding typical regulatory limits by orders of magnitude. Ecotoxicological assessments using *Daphnia magna, Lemna minor*, and *Aliivibrio fischeri* demonstrated severe acute and chronic toxicity, with EC_{50} values for *D. magna* reaching 0.05 %. Even non-ignited, venting modules released significant

* Corresponding author.
E-mail address: krayzell@vscht.cz (L. Pokorna-Krayzelova).

https://doi.org/10.1016/j.watres.2026.126751
Received 23 April 2026; Received in revised form 15 August 2026; Accepted 17 August 2026
Available online 18 August 2026

organic pollutants and exhibited high microbial toxicity. These findings demonstrate that LIB firefighting runoff creates a highly hazardous effluent that matures over time. Specialized on-site containment and pre-treatment are essential to prevent the breakthrough of these toxic elements into the urban sewerage system and the wider aquatic environment.

1. Introduction

Lithium-ion batteries (LIBs) have become the cornerstone technology enabling the global transition toward sustainable transportation and decarbonization of the mobility sector. As the world confronts the urgent challenge of climate change, electric vehicles (EVs) powered by LIBs represent a critical pathway to reducing greenhouse gas emissions from the transportation sector, which accounts for a substantial portion of global carbon dioxide emissions (Bisschop et al., 2020; Sun et al., 2020). The superior energy density, declining production costs, and improving performance characteristics of lithium-ion technology have positioned these batteries as the dominant energy storage solution for modern electric vehicles (Lai et al., 2022; Shahid and Agelin-Chaab, 2022). This technological advancement, coupled with increasingly stringent environmental regulations and government incentives, has catalyzed unprecedented growth in EV adoption worldwide, fundamentally reshaping the automotive industry and offering progress toward international climate commitments (Muratori et al., 2021; Sanguesa et al., 2021).

Following a period of sustained growth, which saw nearly 14 million EVs sold in 2023 (IEA, 2024) and an estimated 17 million units in 2024 (IEA, 2025), the global EV market is projected to continue its robust expansion, with worldwide sales forecast to surpass 20 million units in 2025 (IEA, 2025). This trajectory implies EVs will account for approximately one-in-four (around 25 %) of all new cars sold globally (Zaino et al., 2024), with growth driven primarily by a deepening market in China, where penetration is expected to exceed 50 %, and a policy-driven rebound in Europe (IEA, 2025). This scaling of battery demand extends beyond transportation; global stationary energy storage systems (ESS) are expanding at a comparable pace to stabilize grids relying on renewable energy (Meraner et al., 2026). When these large-scale stationary installations experience thermal failure, they present similar, if not magnified, fire suppression challenges due to the sheer volume of cells aggregated in a single location. This accelerating adoption is further substantiated by the forecast that global EV battery demand will surpass the 1 TWh mark in 2025 (IEA, 2025), cementing the industry's steady march toward mass-market electrification.

Despite their environmental benefits (Alum et al., 2026; Sanguesa et al., 2021), technological advantages (Hammed et al., 2025; Kulkarni et al., 2026), and decreasing production costs (Gouveia et al., 2026), lithium-ion batteries present significant safety challenges that have become increasingly prominent as deployment scales. The high energy density that makes LIBs attractive for automotive applications simultaneously creates inherent risks of thermal runaway, a self-accelerating exothermic reaction that can lead to catastrophic battery failure (Jiaqiang et al., 2024). Thermal runaway can be triggered by multiple mechanisms, including mechanical damage from vehicle collisions or penetration, manufacturing defects such as internal short circuits or contamination, electrical abuse conditions like overcharging or external short circuits, and thermal stress from exposure to elevated ambient temperatures or inadequate cooling (Lu et al., 2013; Ping et al., 2015; Wang et al., 2012). Furthermore, even in the absence of a full thermal runaway event, overheated battery cells may vent toxic and combustible gases, including phosphorus pentafluoride, phosphorus oxyfluoride, and hydrogen fluoride (Larsson et al., 2014; Larsson et al., 2017).

While modern EVs match internal combustion engine vehicles in performance, they represent a radical departure in terms of fire suppression logistics and emergency response. Current emergency response protocols for LIB fires have converged on water-based suppression as the primary intervention strategy, despite significant operational challenges. Water immersion or continuous water application serves multiple functions: cooling the battery pack to temperatures below the thermal runaway propagation threshold, absorbing heat from exothermic reactions, and preventing reignition, which remains a persistent concern due to the stored chemical energy within damaged cells (Mao et al., 2024). Full-scale experimental studies have demonstrated that effective suppression of EV battery fires requires substantial water volumes, with recommendations ranging from 11,000 to 40,000 liters depending on battery size and fire severity, applied over extended periods often exceeding several hours (Cui et al., 2022; Li et al., 2020). The water must be applied continuously or the battery must remain fully submerged for 24 hours or longer to ensure complete cooling and prevent reignition, as damaged cells can spontaneously re-enter thermal runaway even after apparent extinguishment (Cui et al., 2022). Traditional methods, such as foam application, have proven largely ineffective, frequently requiring the physical deconstruction of the battery housing to reach the fire source (Lazarenko et al., 2019; Shen et al., 2024). While existing literature provides extensive data on EV fire behavior and gas-phase emissions (Hynynen et al., 2023; Lecocq et al., 2012; Sturm et al., 2022), there remains a lack of direct focus on the wastewater generated during these incidents.

The reliance on large-volume water suppression for LIB fires introduces a critical yet underexplored environmental dimension to the safety challenges of electromobility. When water contacts burning or thermally damaged battery cells, it facilitates the leaching of hazardous substances from compromised battery components into the aqueous phase, creating contaminated runoff that poses significant risks to soil, groundwater, and surface water ecosystems. Recent large-scale trials by Jalali et al. (2026) have demonstrated that this runoff can contain dissolved metals, fluorinated compounds, and organic pollutants derived from the lithium salts (such as $LiPF_6$, $LiClO_4$, or $LiBF_4$) used in battery manufacturing (Jalali et al., 2026; Nitta et al., 2015; Rensmo, 2022; Xu, 2014). Research by Quant et al. (2023) compared the inorganic and organic pollutant levels of EV extinguishing water against traditional fuel vehicles, testing acute toxicity on *Vibrio fischeri, Pseudokirchneriella subcapitata*, and *Daphnia magna*. While the first two species exhibited high sensitivity, the runoff showed only moderate toxicity toward *Daphnia magna*. Crucially, that study analyzed water collected immediately after suppression without the variable of long-term submersion.

In the current paper, the chemical properties and ecotoxicity of extinguishing water from the lithium-ion vehicle battery fire were investigated. There are studies dealing with the tests with electric vehicle fires (Hynynen et al., 2023; Lecocq et al., 2012; Sturm et al., 2022), however, these studies focus on the gas emissions, rather than wastewater from fire combustion. To the best of our knowledge, this is the first paper dealing with the long-term effect of the EV battery submerged in the water. This paper deals with the temporal dynamics of contaminant leaching during extended submersion periods, the cumulative environmental burden from battery fire incidents, and the ecological effects of battery-derived contaminants in aquatic environments.

2. Materials and methods

2.1. Materials

2.1.1. Large-scale battery fire and submersion experiment

Three Li-ion vehicle batteries (described in Table 1) were fully charged and subsequently ignited. Module A was ignited by short circuit, module B by a repeated mechanical penetration, during which the supervising firefighter struck the module three times with an axe to rupture it, and finally, module C was heated with a hot plate and then pierced by repeatedly. Modules A and B caught visible fire, module B even exploded several times, while module C failed to ignite with only white smoke indicating visible evaporation of the electrolyte solution after the battery rupture.

Although Module B consists of 16 cells arranged in an 8 × 2 configuration compared to the 24-cell arrangements of Modules A and C, its total mass (~30.5 kg) and nominal energy capacity (6.86 kWh) are equivalent to Modules A and C (~30.8 kg). This is due to Module B utilizing larger, higher-capacity individual cells (0.429 kWh/cell vs. 0.286 kWh/cell in A and C) along with heavier internal structural framing. Furthermore, Module B features an NMC 8:1:1 cathode chemistry, which possesses lower thermal stability than the NMC 6:2:2 chemistry of Module A, contributing to the violent combustion and complete physical breakdown observed during its ignition trial.

The vehicle batteries were left to completely burn for approx. 1 hour and immersed in barrel A, B, and C with 230 L of tap water. The experimental vessels used were food-grade, high-density polyethylene (HDPE) barrels previously designated for drinking water storage to ensure chemical inertness; the barrels were thoroughly drained and verified clean, with no standing water left inside prior to the introduction of the experimental matrix. A blank water sample was taken from all three barrels prior to the battery submersion.

Water samples were taken from each barrel over 112 days (three months), using a pristine, unused HDPE sampler. Before taking each sample, the water in the barrels was well mixed and samples were extracted from the middle part of each barrel. The samples were fully analyzed. The complete schedule of sampling and type of samples are shown in Table 2.

From the physicochemical parameters; pH, conductivity, salinity, neutralization capacity, Volatile Suspended Solids (VSS), Total Suspended Solids (TSS), Chemical Oxygen Demand (COD), Dissolved Organic Carbon (DOC), Adsorbable Organically bound Halogens (AOX), bromides, chlorides, fluorides, ammonia nitrogen, nitrites, nitrates, phosphates, sulfates and selected metals were determined in all mixed samples. All samples were filtered through 0.45 μm glass fiber filter (Whatman™) prior the measurements. Each sampling day, a 250 mL of water sample was also taken into the glass sampler for organic analysis. The glass sampler was filled completely with water and closed without headspace to avoid further oxidation. On specific days (see Table 2), samples for ecotoxicity tests were taken as well, together with the samples for physicochemical analysis. Ecotoxicity tests were performed on the following: *Daphnia magna, Aliivibrio fischeri*, and *Lemna minor*. Finally, toxicity to soil organisms was monitored through a dehydrogenase activity (DHA) test, as described below in chapter 2.2.2.

Table 1
The detailed description of Li-ion vehicle batteries.

	Module A	Module B	Module C
Number of cells	24 (12 × 2)	16 (8 × 2)	24
Energy (kWh)	6.86 (24 × 0.286)	6.86 (16 × 0.429)	6.86 (24 × 0.286)
Weight (kg)	30.8	30.5	30.8
Dimensions (mm)	590 × 225 × 108	590 × 225.35 × 108.5	590 × 225 × 108
Nominal voltage (V)	44	29	28
Chemistry	NMC/graphite nickel/manganese/cobalt (6:2:2)	NMC/graphite nickel/manganese/cobalt (8:1:1)	NMC/Alu nickel/manganese/cobalt (8:1:1)

2.1.2. Experimental limitations and matrix considerations

Given the logistical and economic constraints of large-scale vehicle battery destruction testing, this work is framed as a descriptive, single-module exploratory case study (n=1 per ignition condition). Consequently, between-barrel variations are interpreted descriptively rather than through comparative inferential statistics. Tap water was utilized as the baseline matrix, representing typical municipal firefighting water. While tap water contains minor background halides and residual free chlorine (typically 0.2–0.5 mg/L), the potential for chlorine-induced halogenation of organic electrolyte degradation products was minimal. Under the strongly alkaline conditions (pH > 11) generated within 24 hours of submersion, residual chlorine rapidly off-gasses or converts to unreactive species. This was confirmed by AOX monitoring, which remained near detection limits in Barrels A and B. In Barrel C, where organic compounds were most prevalent, AOX peaked early (Day 25) and subsequently declined, showing no cumulative chlorination trend attributable to tap water background chlorine.

Additional environmental factors must be considered when extrapolating these static laboratory barrel results to field conditions: (1) In real-world open containment basins or salvage yards, 3 months of exposure to sunlight, wind, and ambient temperature fluctuations would induce significant water evaporation. This volume reduction would further concentrate mobile pollutants (e.g., Li^+, F^-), resulting in higher pollutant concentrations in residual water than observed in our static, unevaporated barrel setup. (2) While this study models wastewater dynamics for single passenger vehicle modules (~230 L tap water per ~30.8 kg module), large-scale Stationary Energy Storage Systems (ESS) present significantly different water-to-battery mass ratios during suppression. Consequently, while the leaching dynamics and pollutant types are directly transferable, absolute pollutant concentrations from multi-megawatt ESS fires cannot be directly adopted from these vehicle-scale values.

Additionally, for the *Aliivibrio fischeri* bioluminescence assay, the mandatory neutralization (pH 6.8–7.2) and subsequent syringe filtration required to eliminate white haze may have caused the precipitation or adsorption of certain amphoteric metals (e.g., aluminum complexes) and hydrophobic organic compounds. This sample preparation step represents a standard protocol artifact that may lead to a conservative underestimation of the raw effluent's true microbial ecotoxicity.

2.2. Analytical methods

2.2.1. Physico-chemical methods

COD_{Cr} values were determined by the semi-micro method according to ISO 15705 (2002). The decanted samples were mineralized with an oxidizing and catalyst solution for 2 h at a temperature of 150°C in test tubes placed in a thermo-box. The absorbance was measured after cooling the reaction mixture and diluting it with demineralized water at a wavelength of 600 nm in a cuvette with an optical length of 5 cm, the results were calculated from the calibration dependence. COD results were not corrected for halide content beyond standard masking protocols. Chloride interference was mitigated by the addition of Hg^{2+}, whereas the presence of fluorides and bromides was considered to have no significant influence on the analysis due to the negligible reactivity of fluorides and the low concentrations of bromides in the samples. Acid neutralizing capacity (ANC) (ISO 9963-1 (1994), Part 1 and Part 2) were determined in nonfiltered samples by titration with a strong acid (HCl, c = 0.1 mmol/L) with visual indication of the end of the titration using phenolphthalein for carbonate alkalinity $ANC_{8.3}$ (phenolphthalein alkalinity, p-alkalinity) and a mixed acid-base indicator (methyl red,

Table 2
The schedule of sampling campaign.

Sampling Day	1	2	3	4	7	10	14	17	21	28	42	56	84	112
Mixed sample	✓	✓	✓	✓	✓	✓	✓	✓	✓	✓	✓	✓	✓	✓
Sample for Ecotoxicity tests	✓				✓					✓		✓	✓	✓

bromocresol green) for alkalinity $ANC_{4.5}$ (total alkalinity, m-alkalinity). Each sample was carefully titrated in triplicates. The concentration of bromides was determined spectrophotometrically using the phenol red method (APHA, 2012). The method is based on the oxidation of bromides present in the sample with chloramine-T and subsequent bromination of phenol red. The concentration of fluorides was determined spectrophotometrically using the SPADNS method (APHA, 2012). The method is based on the reaction of fluorides with Zr^{4+} in the acid environment. The non-colorful complex ZrF_6^- reacts with SPADNS and creates red colored complex depending on the concentration of fluorides.

2.2.2. Ecotoxicity tests

All ecotoxicological results are expressed as a percentage (%), representing the volume-based concentration (v/v) of the wastewater sample within the test medium. These values indicate the degree of dilution of the effluent required to achieve the calculated EC50 or EC20 endpoints.

Testing of the samples for *Aliivibrio fischeri* bacteria was carried out in accordance with ISO 11348-2. This test is designed to detect the inhibition of natural bioluminescence of the bacteria by measurement in a luminometer. The samples had very high pH values and prior to the determination it was necessary to adjust them with HCl to pH values between 6.8 and 7.2. Samples had to be filtered through a syringe filter after pH adjustment due to white haze formation. All samples were then salinized to account for the relatively high conductivity, resulting in a salinity of 2 %. Screening tests were carried out first. Based on the results of these tests, concentration ranges were determined for each sample to establish an EC_{50} value. For all samples, the concentrations tested ranged between 16.6 and 80 % (v/v). Liquid-dried bacteria (LCK 482, Hach Lange, GmbH) were revitalized with a special solution and kept at 15°C in a thermo-block throughout the test. The samples were diluted and a minimum of 5 concentrations were tested each time, with the highest concentration tested being 80 % where appropriate. The control (2 % NaCl solution only), samples and standard (Zn^{2+} solution) were measured in sequence using a luminometer after 15 and 30 minutes of exposure to the bacteria. Tests were performed in triplicate. From the results obtained, the EC_{50} or EC_{20} values were calculated, representing the concentration (v/v) that causes a 50 or 20 % reduction in bioluminescence.

Duckweed assay was conducted according to ISO 20079 using *Lemna minor* L., strain Steinberg (FDA, Berlin, Germany). Steinberg medium modified by Altenburg (pH 5.5 ± 0.2) was chosen as control and dilution medium to achieve a concentration rate of samples. Growth rate was based on total frond area that was determined using image analysis NIS Elements (Version 5.20, Laboratory Imaging, Prague, Czech Republic). After 7-day-exposition the total chlorophyll was determined by extraction in pure methanol (24 h; 4°C, dark) followed by spectrophotometry (Shimadzu UV-1900, Japan). The calculation of the pigment content per frond area was made according to Wellburn (1994).

Determination of *Daphnia magna* inhibition was carried out according to the standard EN ISO 6341 (2012). The same artificial medium (ADaM, see composition in Supplementary Materials) was used for both daphnia hatching and the assay itself. The pH of the prepared medium was adjusted to 7.5 ± 0.5 using 1M hydrochloric acid and 1M sodium hydroxide solution. The test solutions were added to 100 mL beakers and young daphnids (aged less than 24 hours) were transferred using a Pasteur pipette, 5 per beaker. The daphnia were not fed or aerated during the test. After 24 h and 48 h, immobilization of daphnia was recorded. The validity of the test was verified using controls where no more than 10 % immobilization could occur. All measurements were performed in four repetitions. Probit analysis was used to interpret the ecotoxicological tests. A log(concentration) probit regression model was used to calculate slopes and intercepts. The Microsoft Excel software was used for the calculation of the LC_{50} values and fiducial confidence intervals at 0.05 level of significance.

Soil dehydrogenase activity (DHA) was measured after application of liquid samples into two types of standard soils (Lufa Speyer, Germany) according to ISO 23753-1. Lufa soil type 2.2 is characterized as a sandy loam soil with an organic carbon content (TOC) of 1.61±0.44 %, pH (0.01 M $CaCl_2$) of 5.6±0.4, cation exchange capacity (CEC) of 85±121 meq/kg and maximum water-holding capacity (WHCMAX) of 433±51 g/kg. Lufa soil type 2.4 is characterized as a loam soil with TOC of 1.95 ±0.25 %, pH (0.01 M $CaCl_2$) of 7.4±0.1, CEC of 212±151 meq/kg and WHCMAX of 458±27 g/kg. Soils were air-dried at laboratory temperature, contaminated with samples to 50 % WHC and incubated in glass vessels covered with aluminum foil at 20±1°C. Samples of contaminated soils were air-dried for soil pH determination according to ISO 10390 using 0.01 M $CaCl_2$. After seven days of incubation, DHA was conducted. All parameters measured in samples were expressed as percentage of inhibition (immobilization) in comparison with control. No observed effect concentration (NOEC) and the lowest observed effect concentration (LOEC) were determined via Dunnett test using GraphPad Prism SW. EC_{50} with 95 % confidence interval was calculated based on inhibition data via nonlinear regression using GraphPad Prism (Version 10.2, Boston, MA, USA).

The overview of all standard procedures used for the analysis is described in Table 3.

2.2.3. Instrumental methods

The pH value of the samples was determined using a desktop pH meter InoLab pH level 2 (WTW GmbH & Co, Germany) with combined pH electrode HC 173-FES (THETA 90, Czech Republic), and the specific conductivity was measured with an InoLab Cond 740 instrument (WTW GmbH & Co, Germany).

Concentrations of selected metals (Li, As, Cr, Zn, Sb, Cd, Pb, Ni, Mn V, Ca, Cu, Na, K, Tl, Al, Ba, Be, Co, Fe, Mg, Mo, Se, Sn, Sr, Ti) were determined with ICP-OES instrument, Perkin Elmer- Optima 2000DV (PerkinElmer, Massachusetts, USA). This device consists of a peristaltic pump, a nebulizer, a double monochromator, a CCD detector and a plasma head with an induction coil. It is a dual spectrometer, which means that it enables double, axial and radial observation of the discharge. The PerkinElmer-Optima 2000 DV uses a spectral region between 160-900 nm, and the detection limit is 10 μg/L.

Table 3
The summary of all used standard methods and international standard operational procedures (ISO).

Analyte	Type of parameter/assay	ISO
COD_{Cr}	Physico-chemical parameter	ISO 15705 (2002)
ANC	Physico-chemical parameter	ISO 9963-1 (1994)
Bromides	Physico-chemical parameter	Standard Methods 4500-Br-B
Fluorides	Physico-chemical parameter	Standard Methods 4500-F-D
AOX	Physico-chemical parameter	ISO 9562 (2004)
Aliivibrio fischeri	Fresh water assay	ISO 11348-2
Daphnia magna	Fresh water assay	ISO 6341
Lemna minor	Fresh water assay	ISO 20079
DHA	Functional microbial assay	ISO 23753-1

Na and K concentrations were measured using a SavantAA atomic absorption spectrometer (GBC Scientific Equipment, Australia) with a continuous source of radiation, which enables hyperpulse background correction. Furthermore, this apparatus consists of a Festie-Elbert grating monochromator, a universal photomultiplier, an atomizer and a hollow-cathode discharge lamp.

The analysis of nitrite, nitrate, ammonia nitrogen, phosphate, sulfate, and chloride were done by the Thermo Scientific™ Gallery™ Analyzer (Thermo Fisher Scientific, Massachusetts, USA).

AOX were determined by LTX-2000 (LABTECH Ltd., Czech Republic) according to the ISO 9562 (2004). During the procedure, a shaking method was used and to achieve the desired pH value < 2, it was necessary to add 1-2.5 mL of concentrated HNO_3 per 100 ml of sample, due to its buffering capacity. The uncertainty of determination is 10 %. The standard addition method was used to verify possible interferences.

X-ray fluorescence (XRF) was used for the elemental analysis of the solid particles in the samples. A 250 ml sample was filtered through 0.45 μ membrane filter, and dried. Filters with suspended solids were analyzed directly using ED-XRF ElvaX Mobile. For the analysis, dual task method with usual task 35 kV, 10 μA 20 seconds (pre-filter Al-800 μm) and Light task 12 kV, 50 μA, 80 seconds (without pre-filter) were used.

Organic compounds were analyzed using Gas chromatography–mass spectrometry (GC-MS). Water samples for GC-MS analysis were filled into 250 mL glass bottles with GL-45 caps without headspace. Samples of organic compounds were collected by thin-film solid-phase microextraction (TF-SPME) membranes submerged into water samples for 15 minutes during continuous stirring of samples on magnetic stirrer (at laboratory temperature). After 15 minutes TF-SPME membranes were rinsed with demineralized water and dried and then transferred into Markes thermal desorption tubes and desorbed in Markes thermal desorption system TD100-XR and analyzed at GC-MS system Agilent 5977C MSD with Agilent 8860 GC. Because TF-SPME provides semi-quantitative peak-area profiles, GC-MS results are interpreted based on detection frequency and temporal trends rather than absolute concentrations.

Vario EL Cube (Elementar GmbH, Germany) was used for the simultaneous determination of carbon, hydrogen, nitrogen and sulfur. The analyzer is equipped with a TCD detector and additionally IR detector which is used for determination of the low sulfur content (below 100 ppm). Simultaneous C, H, N, S determination is based on high-temperature (up to 1200°C) combustion of the analyte in the oxygen stream. Gaseous products of combustion (N_2, CO_2, H_2O a SO_2) are purified, separated and finally determined by TCD. Typical samples are organic chemicals, but many inorganic compounds can be analyzed as well.

Fully automatic sequential XRF - spectrometer Axios (PANanalytical, Holland) was used for qualitative and quantitative element analysis. The spectrometer is equipped with Rh tube, 4kW generator, 3 collimators, 8 crystals (PX1, PX4a, PX5, PX7, PE002, Ge 111, LiF 200, LiF 220), and 2 detectors – proportional and scintillation.

Detailed analytical quality control parameters, including instrument-specific limits of detection (LODs), standard measurement uncertainties, method recoveries, and matrix validation protocols, are comprehensively documented in Table S1 of the Supplementary Materials S1.

3. Results

Since the battery of module A was ignited by a short circuit, it was not completely damaged, unlike the battery of module B, which needed repeated breakthroughs for complete ignition, resulting in strong damage. Module C was destroyed partially. The type of ignition and subsequent destruction of the battery type played a crucial role in the final battery condition (Fig. 1). The destruction of modules could be ordered as: module A (almost untouched, slight burn), module C (mildly burned on the outside from hot plate, evaporated electrolyte), and module B (completely destroyed by blasts as well as by the fire). For this reason, also the submerging wastewater composition in the barrels looked different. The TSS from module A was around 11.6 g/L, the TSS of module B was more than twice higher, approx. 29.7 g/L, and TSS of module C was low (approx. 0.9 g/L). However, despite the high difference between the TSS, the VSS of mixed samples was very similar and reached 3.9, 2.4 and 2.4 mg/L in barrels A, B, and C, resp. after 112 days.

3.1. Mixed samples

The wastewater from battery fires, module A, B and C, reached very similar pH values (11.3, 11.4, and 12.4, resp.), conductivity of module A, and B were high (22.5 and 23.1 mS/cm, resp.), while in module C, it reached only 5.7 mS/cm. While the increase of pH was practically immediate and reached the final value the first day after the battery submersion in all barrels, the conductivity was slowly but constantly increasing in barrels A and B until it reached stable value (plateau) on day 84 (more precisely somewhere between day 56 and 84). In barrel C, stable value in case of conductivity was never reached and kept increasing (Fig. 2, 1**C**).

The COD fluctuated over the complete 112 days with a maximum of 72 and 123 mg/L for A and B, resp. COD of module C was continuously increasing from 112 mg/L on day 1 to more than 500 mg/L on the last day of sampling. A similar trend followed the AOX analysis, while in module A and B, the value did not exceed 20 μg/L in all samples analyzed, in module C, the AOX reached peak up to 900 μg/L on day 25 and then decreased to 10-30 μg/L on the last days (AOX data not shown). The value of alkalinity $ANC_{4.5}$ was slow but constantly increasing in barrels A and C (Fig. 2, 1**A-1C**). In barrel A, it did not even reach stability (with max. of 174 mmoL/L in day 112). In barrel B, stability in alkalinity $ANC_{4.5}$ (189 ± 3 mmoL/L) was reached approx. after 5 days. In barrel C, the alkalinity was much lower compared to A and B but constantly increasing without stabilization until the very last day of sampling. The course of $ANC_{8.3}$ was similar in all barrels, constantly increasing throughout the 112 days, however in barrel C, the value was significantly lower.

In terms of halides, bromides and fluorides were measured in the water samples (Fig. 2, **2A-2C**). Bromides appeared in the barrels in all three cases after 21 days and their concentration was around 0.8, 3.6

Fig. 1. Vehicle batteries after ignition (before submerging into the barrel with water). Left – module A (ignited by short circuit, visible but small fire, no blasts), Middle – module B (ignited by repeated breakthrough, complete destruction, heavy fire, several blasts), Right – module C (heated by hot plate and ignited by repeated breakthrough, without visible fire, only white smoke release).

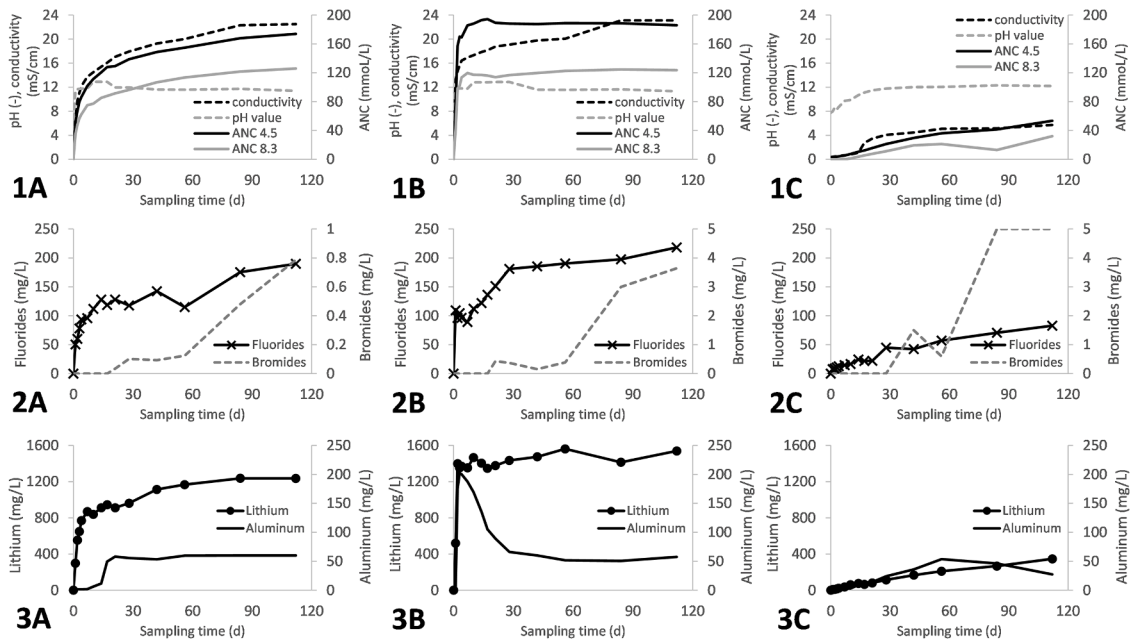

Fig. 2. The concentration of selected parameters in submersion experiment: conductivity, pH value, $ANC_{4,5}$, and $ANC_{8,3}$ (1A – for module A; 1B – for module B, 1C – for C module); fluorides and bromides (2A – for module A; 2B – for module B, 2C – for C module); and Lithium and aluminum (3A – for module A; 3B – for module B, 3C – for C module). Note the different second axes of 2A compared to 2B and 2C.

and 5.0 mg/L after 112 days for modules A, B and C, resp. (Table 4). The concentration of fluorides was increasing throughout the entire sampling period and reached 190 mg/L in barrel A, 218 mg/L in barrel B, and 82.7 mg/L in barrel C (Table 4). The concentrations of chlorides were basically stable in all barrels and were approx. 25.2 ± 3.6 mg/L in barrel A, 39.4 ± 6.1mg/L in barrel B, and 24.7 ± 2.2 mg/L in barrel C (chloride data not shown).

The concentration of nitrites, nitrates, ammonia nitrogen, phosphates and sulfates were also measured in all barrels. The final concentrations of these parameters on day 112 are published in Table 4 together with their corresponding change (increase, decrease or stable value). While phosphate and nitrate decreased in all barrels, ammonia nitrogen and sulfate were mainly increasing (except for sulfate in barrel C). Nitrite was close to the detection limit in all barrels.

The complete metal analysis showed the biggest difference between all three barrels and vehicle batteries. The highest concentration was measured for lithium in all barrels (Fig. 2, 3**A**-3**C**). The concentration was increasing during the whole 3 months and reached 1.24 g/L in barrel A, 1.54 g/L in barrel B, and 0.35 g/L in barrel C. From other metals, aluminum played an important role in all barrels, however its concentration evolved differently (Fig. 2, 3**A**-3**C**). While in barrel A, the concentration of aluminum reached approx. 50 mg/L within 17 days and stabilized, its concentration in barrel B sharply increased to 200 mg/L in 4 days and then was decreasing until it reached approx. 60 mg/L between days 28-42. In barrel C, the concentration of aluminum reached 50 mg/L on day 56 and partially decreased to 35 mg/L at the end of experiment. Other metals that showed certain values (below 1 mg/L) but were not on the edge of the detection limit (0.01 mg/L) were Zn, Ca, Cu, Ba, Na and K for barrel A, Ca, Cu, Ba, Na and K for barrel B, and Ca, Cu, Ba, Mg, Na and K for barrel C.

GC-MS screening revealed scenario-specific semi-quantitative temporal patterns in the appearance and disappearance of organic compounds across the three barrels (**Tables S2–S4**). Volatile aromatics such as benzene, toluene, ethylbenzene, and xylenes were consistently detected on day 1 in all barrels, but their presence declined rapidly: benzene disappeared after day 1 in barrels A and B and after day 42 in barrel C, while toluene persisted longer, appearing on 7–8 sampling days in barrel B and up to day 84 in barrel C. Mid-period samples (days 3–28) showed increasing frequency of oxygenated compounds such as 1-butanol and benzaldehyde, which appeared on 6–8 sampling days, indicating secondary formation during submersion. Heavy alkanes exhibited strong late-period persistence: barrel B contained the broadest range, with C17–C32 alkanes detected on 4–5 separate sampling days, including triacontane (C30) and dotriacontane (C32) by day 56. Barrel A

Table 4
Concentration of selected parameters on first day (1) and last day (112). The arrow indicates the decreasing or increasing values over the whole experiments ("↓" = decreasing trend, "↑" = increasing trend, "~" = same value, "↑↓" = first increase followed by decrease).

	unit	Barrel A			Barrel B			Barrel C		
	day	1	112		1	112		1	112	
Sulfate	mg/L	13.3	225.3	↑	229.3	340.1	↑	40.2	7.9	↓
Phosphate	mg/L	0.2	0.1	↓	1.1	0.6	↓	1.6	3.1	↑
Nitrite	mg/L	< 0.1	0.3	↑	< 0.1	< 0.1	~	< 0.1	< 0.1	~
Nitrate	mg/L	6.1	2.5	↓	6.5	5.2	↓	4.6	0.7	↓
Ammonia nitrogen	mg/L	0.1	6.6	↑	BDL	5.9	↑	0.1	0.8	↑
Fluoride	mg/L	50.5	189.8	↑	109.3	218.2	↑	7.8	82.7	↑
Bromide	mg/L	BDL	0.8	↑	BDL	3.6	↑	BDL	5.0	↑
Chloride	mg/L	26.1	26.4	~	32.3	32.0	~	26.2	28.7	~
AOX	µg/L	BDL	16	↑	BDL	BDL	~	33	15	↑↓

BDL = below detection limit

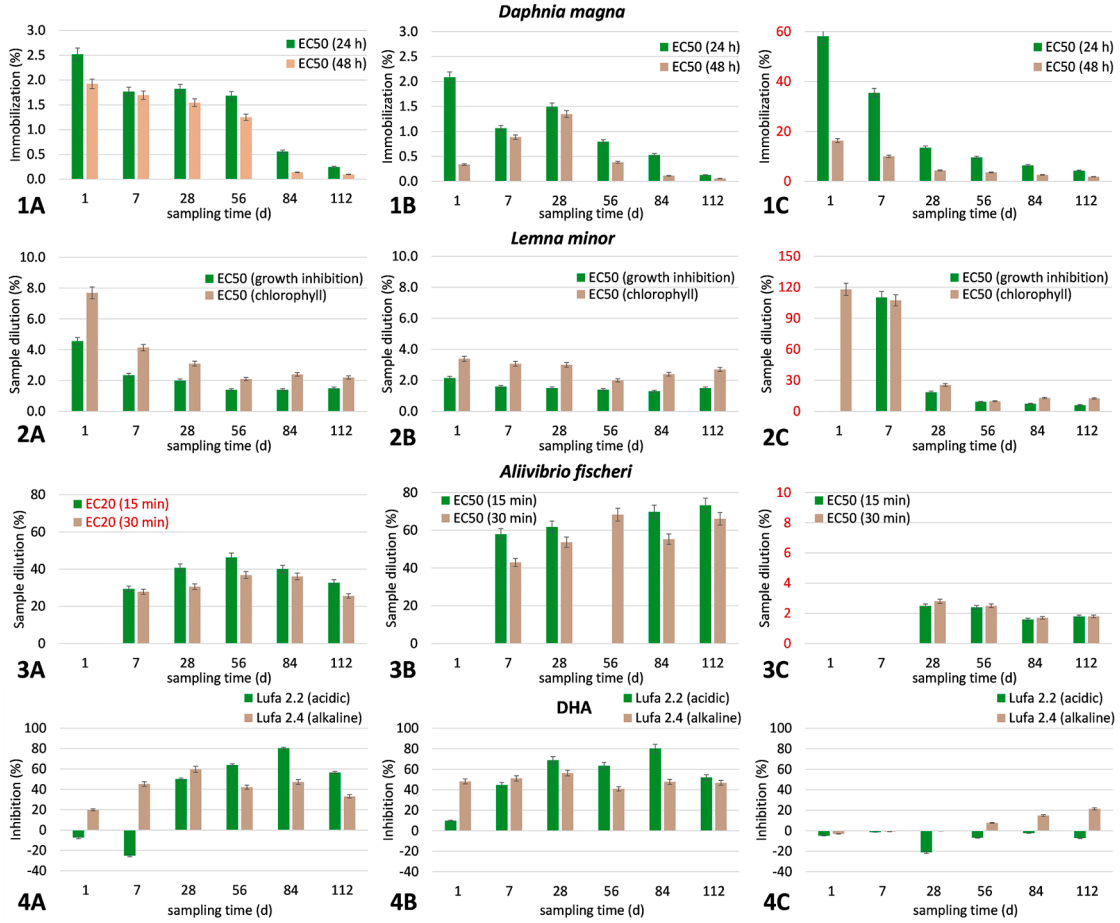

Fig. 3. The results of EC_{50} during ecotoxicological tests: *Daphnia magna* (1A for barrel A, 1B for barrel B, 1C for barrel C); *Lemna minor* (2A for barrel A, 2B for barrel B, 2C for barrel C), *Aliivibrio fischeri* (3A for barrel A, 3B for barrel B, 3C for barrel C), and DHA (4A for barrel A, 4B for barrel B, 4C for barrel C). For *Aliivibrio fischeri* in barrel A (3A), only EC_{20} was detectable. Note the different Y axes for (1C, 2C, and 3C).

showed fewer heavy alkanes, mostly appearing only in late samples (days 42–56), while barrel C lacked heavy alkanes entirely and instead exhibited long-term presence of oxygenated heterocycles such as 2-methylfuran, 2,5-dimethylfuran, and 2-acetyl-5-methylfuran, each detected on 6–8 sampling days. Persistent compounds such as 2-ethyl-1-hexanol and benzothiazole appeared in nearly every sampling day across all barrels (7–10 occurrences), demonstrating high stability or continuous release. Late-period samples (days 84–112) showed a shift toward more complex structures, including phenolic derivatives and small acids (e.g., m-cresol and acetic acid), consistent with progressive electrolyte degradation. A complete list of compounds and detection frequencies is provided in **Supplementary Material S2 (Tables S2–S4)**.

Finally, after the filtration of wastewater, all the filters were analyzed by XRF. The results showed very strong composition of practically all components. The TSS composition of barrels A and B was very similar, while barrel C slightly diverged indicating that it plays a crucial role if the battery catches fire or not. The list of emitted elements with high concentration were Al, Cl, Si, P, Ca, K, Mn, Co, Ba, Zn, Ni and Cu. **Figure S1** with all mentioned crucial parameters displayed can be found in Supplementary material S2.

3.2. Ecotoxicity tests

The ecotoxicological evaluation revealed significant differences in toxicity profiles among the three tested barrels A, B, and C across different trophic levels (Fig. 3). Barrels A and B exhibited the highest acute and chronic toxicity toward higher organisms. In *Daphnia magna* (water flea) assays (Fig. 3, 1**A-**1**C**), both samples showed extreme toxicity, with barrel B being the most potent; by day 112, its EC_{50} (48h) reached a critical value of 0.05 %, followed closely by barrel A at 0.09%. A similar trend was observed in *Lemna minor* (duckweed) assays (Fig. 3, 2**A-**2**C**), where growth inhibition (frond multiplication) proved to be a more sensitive endpoint than chlorophyll degradation (Fig. 4). For instance, on day 112, barrel A reached an EC_{50} for growth of approximately 1.5 %, while the EC_{50} for chlorophyll was 2.2 %, suggesting that the leached contaminants primarily suppress biomass production rather than causing immediate photosynthetic pigment breakdown (additional data on chlorophyll and growth of *Lemna minor* can be found in Supplementary material S3, **Figure S2**).

In contrast, barrel C displayed a delayed toxicity profile and a unique target range. While it was the least toxic to crustaceans and plants, it proved to be the most hazardous to microbial communities. This was evidenced by the *Aliivibrio fischeri* bioluminescence assay (Fig. 3, 3**A-**3**C**), where barrel C reached a high toxicity level with an EC_{50} of 1.8 % at day 112. Conversely, barrels A and B had a much lower impact on these marine bacteria, with barrel B showing an EC_{50} of only 73.3 % and barrel A showing no measurable EC_{50} within the tested range. Interestingly, barrel C initially exhibited a hormetic effect on *Lemna minor*, where low-dose exposure stimulated growth before cumulative leaching led to toxicity.

Fig. 4 illustrates the temporal phenotypic response of *Lemna minor* exposed to wastewater from barrels A, B, and C, compared to the control group. Wastewater from all three barrels induced progressive chlorosis and tissue necrosis. Barrel A exhibited the most rapid onset of toxicity, with significant bleaching observed as early as day 28. In contrast, barrels B and C demonstrated a slower rate of pigment degradation,

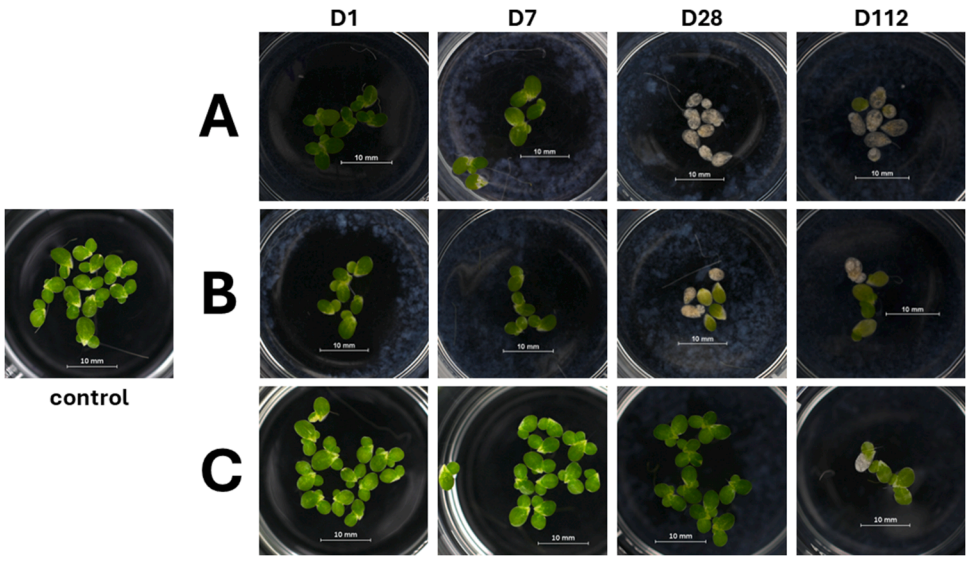

Fig. 4. Time-course progression of chlorosis and tissue decay in *Lemna minor* exposed to wastewater from barrels A, B, and C, compared to control conditions. Images captured at days 1, 7, 28, and 112 illustrate the impact of the wastewater from each barrel on pigment stability and plant viability. Scale bars: 10 mm.

suggesting a lower initial phytotoxicity; however, by day 112, all treated cultures showed signs of advanced decay. These observations indicate a time-dependent negative impact of the wastewater on the physiological stability of *Lemna minor*, with the severity of the response varying according to the treatment source.

The assessment of soil health via Dehydrogenase Activity (DHA) inhibition further differentiated the samples (Fig. 3, 4**A**-4**C**). DHA serves as a key indicator of the overall metabolic activity of soil microorganisms. Data from the DHA inhibition tests (conducted on acidic Lufa 2.2 and alkaline Lufa 2.4 soils) indicated that barrel A and barrel B caused substantial metabolic suppression, with inhibition levels often exceeding 50–80 % as leaching progressed. Interestingly, in the early stages, these samples occasionally showed negative inhibition (stimulation), suggesting a transient hormetic effect or nutrient input before the toxic components reached critical concentrations. Barrel C, however, maintained a much lower impact on soil DHA, with inhibition values remaining close to zero or even showing slight stimulation in some cases, confirming that its primary toxic impact is aquatic-specific rather than soil-metabolic. Overall, a consistent temporal trend was observed across all tests: toxicity significantly increased over the 112-day period, indicating a progressive leaching of bioavailable toxic substances from the source materials.

4. Discussion

4.1. Influence of battery destruction on wastewater composition and pollutant load

While a static 112-day submersion regime differs significantly from the immediate, high-flow operational phase of active fire suppression, these experimental conditions are highly representative of real-world post-incident logistics. Under current emergency protocols, severely damaged or burned EVs may be transported to salvage yards, open containment areas, or specialized quarantine zones where they may be left exposed to precipitation or intentionally submerged in retention basins for extended periods to prevent delayed chemical reignition. The water-to-battery mass ratio used here acts as a boundary case study to model the long-term leaching kinetics and chemical “maturation” of trapped runoff within confined containment environments.

However, two critical operational factors limit the direct extrapolation of these baseline concentration values to all field scenarios: (1) In an unsealed, open-air containment basin, 3 months of exposure to solar radiation, wind, and ambient temperature fluctuations would lead to substantial water evaporation. Because key inorganic contaminants such as lithium (1.54 g L^{-1}) and fluorides (218.2 mg L^{-1}) as well as heavy organic residues do not volatilize at ambient temperatures, water loss would drive a sharp increase in contaminant concentrations in the residual pooled water beyond the values reported in this static, unevaporated trial. (2) While the deployment of stationary ESS in renewable energy grids presents magnified fire suppression hazards due to massive cell aggregations, the water-to-battery mass ratio during an ESS incident is fundamentally different from a single passenger vehicle fire. ESS fires typically demand extended, high-volume deluge cooling over tens of hours, altering the dilution dynamics. Consequently, while the qualitative leaching dynamics, inorganic pathways, and toxicological risks identified here apply universally to lithium-ion chemistry, the exact wastewater concentrations from ESS fires cannot directly adopt the absolute quantitative values measured in this single-vehicle module study.

The degree of destruction during LIB fire critically determines the composition and pollutant load of firefighting wastewater, as demonstrated by the marked differences observed among the three experimental modules in this study. Module B, which underwent complete destruction with heavy fire and several blasts following repeated breakthrough ignition, consistently exhibited the highest concentrations of contaminants across nearly all measured parameters. In contrast, barrel A (ignited by short circuit with small visible fire and no blasts) and barrel C (heated by hot plate with repeated breakthrough ignition, producing only white smoke without visible fire) showed substantially lower pollutant loads, though still environmentally significant.

The relationship between thermal runaway severity and contaminant release is well-established in the literature. Quantitative chamber tests of prismatic nickel-rich cells have shown that thermal runaway emissions can account for approximately 28.5 % of total cell mass, with substantial settleable particles and numerous elemental species detected (Zhang et al., 2019). Severe thermal runaway events produce large particulate loads and multi-phase emissions including gases, soot, and settleable particles, thereby increasing the pollutant mass captured in runoff and extinguishing water (Quant et al., 2023; Zhang et al., 2019). In contrast, minor fires or surface soot deposition tend to leave mainly soot and metal-oxide surface contamination, which transfers into water at lower mass loads than full cell rupture and combustion (Sturm et al., 2022).

In the present study, module B's complete destruction resulted in

lithium concentrations reaching 1.5 g/L, fluoride concentrations up to 218 mg/L, and conductivity values approaching 20 mS/cm; levels comparable to landfill leachates (Benaddi et al., 2022). These extreme values reflect the extensive breach of cell integrity, allowing maximum contact between internal battery components (cathode materials, electrolyte, separator, and current collectors) and the immersion water. The prolonged 112-day submersion period further facilitated continuous leaching of soluble species and gradual dissolution of less-soluble metal oxides and fluoride compounds. Barrel A, despite experiencing visible fire, maintained greater structural integrity, resulting in intermediate pollutant concentrations. Barrel C, characterized by white smoke release without visible flames, demonstrated that even thermal events without overt combustion can release significant quantities of contaminants, particularly volatile and semi-volatile organic compounds and fluoride species from electrolyte decomposition. Semi-quantitative GC-MS detection frequencies (**Tables S2–S4**) confirm that heavily damaged modules released the broadest range of persistent organics, while venting modules produced long-lasting oxygenated heterocycles. However, the detection of aromatic hydrocarbons (benzene, toluene, ethylbenzene, xylenes), aldehydes (benzaldehyde, nonanal), alcohols (1-butanol, 2-ethyl-1-hexanol), alkanes, benzothiazole, and sulfur dioxide across all three modules (with varying temporal patterns) underscores that organic pollutant profiles are influenced by both combustion intensity and thermal decomposition pathways.

Studies extrapolating measured runoff concentrations from large-scale battery fire incidents indicate potential exceedance of ecological thresholds, with environmental hazard potential rising proportionally with incident scale (Quant et al., 2023). The present findings confirm that firefighting operations involving severely damaged battery modules generate wastewater streams requiring specialized containment and treatment protocols, as uncontrolled discharge could pose severe risks to aquatic ecosystems.

4.2. Relation between wastewater contaminant and battery construction

The high concentrations of lithium, fluoride, cobalt, nickel, manganese, and aluminum observed in the firefighting wastewater are directly attributable to the specific construction and chemical composition of NMC LIBs used in electric vehicles. Understanding the source-to-contaminant mapping is essential for predicting pollutant profiles and designing targeted treatment strategies.

Lithium originates from two primary sources within the battery: the layered NMC cathode active material ($LiNi_xCo_yMn_zO_2$, where x+y+z=1) and the electrolyte salt lithium hexafluorophosphate ($LiPF_6$) dissolved in organic carbonate solvents (typically dimethyl carbonate, diethyl carbonate, and ethylene carbonate) (Pražanová et al., 2023). Both lithium sources are highly water-soluble or readily mobilized through electrolyte leakage and hydrolysis reactions (Pražanová et al., 2023). The observed lithium concentrations up to 1.5 g/L in barrel B (and 1.2 g/L in barrel A) wastewater reflect extensive dissolution of both cathode-bound lithium and electrolyte-derived lithium salts. The significantly lower concentration of lithium in barrel C (0.35 g/L) might be only from electrolyte-derived lithium salts since there was no visible harm to the battery itself.

Fluoride contamination arises predominantly from the decomposition and hydrolysis of $LiPF_6$ electrolyte, fluorinated solvents, and polyvinylidene fluoride (PVDF) binder used in electrode fabrication and separator materials (Pražanová et al., 2023; Xu, 2014). The hexafluorophosphate anion (PF_6^-) is highly susceptible to hydrolysis, particularly under elevated temperatures and in the presence of moisture, producing hydrofluoric acid (HF) and lithium fluoride (LiF) according to the reaction: $LiPF_6 + H_2O \rightarrow LiF + POF_3 + 2HF$ (Pražanová et al., 2023; Xu, 2014). Thermal and oxidative decomposition during fire events further accelerates fluoride release from PVDF binder and separator materials (Ping et al., 2015; Xu, 2014). The measured fluoride concentrations up to 218 mg/L in this study are consistent with extensive electrolyte hydrolysis and polymer decomposition in barrel B.

Cobalt, manganese, and nickel are transition metals integral to the NMC cathode active material structure. In NMC chemistries, these metals occupy octahedral sites within the layered lithium metal oxide lattice, providing the electrochemical activity necessary for battery function (Aaltonen et al., 2017; Pražanová et al., 2023). During thermal events and prolonged water immersion, these metals are mobilized through several mechanisms: (1) acidic chemical leaching facilitated by HF generated from electrolyte decomposition, which aggressively dissolves layered NMC oxides (Aaltonen et al., 2017); (2) thermal and oxidative decomposition that converts structural metal oxides into more soluble forms (Ping et al., 2015); and (3) mechanical fragmentation and surface exposure that increases reactive surface area, particularly for moisture-sensitive nickel-rich NMC materials (Geldasa et al., 2022). Detailed pre-recycling analyses of NMC622 pouch cells have confirmed $LiNi_{0.6}Co_{0.2}Mn_{0.2}O_2$ cathode composition on thin aluminum current collectors, identifying these components as primary sources for transition metals in aqueous extracts prior to thermal modification (Pražanová et al., 2023). Acid-reducing leaching studies of spent lithium-ion battery electrode powders – specifically utilizing mineral acids like 2 M sulfuric acid or 4M hydrochloric acid with a hydrogen peroxide reducing agent– have demonstrated high extraction yields, with cobalt typically appearing most concentrated, followed by minor quantities of nickel and manganese (Aaltonen et al., 2017). In our study, all three metals stayed in the form of suspended solids and were not detected in the liquid phase. However, this introduces a distinct environmental pathways risk. If this untreated wastewater is discharged directly into surface waters, these metal-bearing solid particles will inevitably settle. Once embedded in aquatic sediments, changes in ambient environmental conditions – such as localized acidification, shifts in redox potential, or microbial activity – could remobilize these toxic transition metals into bioavailable ionic forms (Co^{2+}, Ni^{2+}, Mn^{2+}), presenting a severe, long-term secondary ecotoxicological hazard to benthic communities.

The difference in NMC cathode stoichiometry (NMC 8:1:1 in Module B vs. NMC 6:2:2 in Module A) significantly influenced cell integrity during fire exposure. High-nickel cathodes (8:1:1) undergo greater structural degradation at elevated temperatures, accelerating physical cell fragmentation upon breach. Although transition metals (Ni, Mn, Co) remained in the solid particulate phase (TSS) without significant dissolution into the bulk liquid due to high ambient pH (11.3–12.4), the higher initial nickel and cobalt content in Module B generated a higher concentration of metal-laden particulate matter in runoff. If discharged without sediment filtration, these settled particles pose a localized secondary hazard upon long-term environmental weathering in aquatic sediments.

Aluminum contamination originates primarily from the thin aluminum foil used as the cathode current collector, with additional contributions from aluminum-containing cell casings and structural alloys (Aaltonen et al., 2017; Pražanová et al., 2023). The observed aluminum concentrations, peaking at approximately 50 mg/L in the wastewater, are primarily governed by the metal's amphoteric nature under the highly alkaline conditions (pH 11–12) generated during battery submersion. In this pH range, aluminum does not precipitate as a solid hydroxide but instead forms a highly soluble aluminate complex, $[Al(OH)_4]^-$ (Mukhamed'yarova et al., 2021). This explains the sustained presence of dissolved aluminum in the alkaline environment. The stabilization of these levels around 50 mg/L suggests a state of chemical equilibrium, likely influenced by the simultaneous leaching of lithium and fluorides, which may trigger the formation of secondary minerals such as Lithium-Aluminum Layered Double Hydroxides (LDHs) (Hoban et al., 2025). Consequently, while the wastewater may appear clear, it carries a high "latent" solids load that would rapidly precipitate as a gelatinous hydroxide floc if the pH were neutralized, posing significant challenges for downstream wastewater treatment and aquatic toxicity management (Krupińska, 2020).

The delayed appearance of **bromide** ions suggests that this species

originates from the degradation of auxiliary battery components rather than the active cell chemistry. Brominated flame retardants (BFRs), commonly found in the structural plastics, connectors, and printed circuit boards of the battery pack, undergo thermal decomposition during the fire event (Watanabe and Sakai, 2003). The subsequent rise in bromide concentration during the submersion period indicates a diffusion-controlled leaching process. This leaching is likely exacerbated by the highly alkaline environment (pH > 11), which promotes the hydrolysis of brominated organic compounds, effectively mobilizing Br^- into the aqueous phase.

Additional elements detected in this study (including calcium, potassium, barium, zinc, copper, silicon, phosphorus, and chloride) likely originate from secondary battery components (casings, terminals, electronic control modules), manufacturing residues, and impurities in raw materials. The comprehensive elemental profile observed in barrel B wastewater reflects the complex multi-material construction of modern electric vehicle battery modules.

4.3. Ecotoxicological impacts

The ecotoxicity profiles documented across all trophic levels represent the cumulative impact of chemical mixtures. In environmental toxicology, complex effluents frequently exhibit synergistic toxicity, where the co-presence of organic electrolyte solvents, volatile aromatic hydrocarbons, fluorides, and metals creates a significantly higher toxic hazard than would be predicted by summing individual compound thresholds.

The severe ecotoxicity observed in this study for *Daphnia magna* and *Lemna minor*, along with measurable effects on *Aliivibrio fischeri*, can be interpreted in the context of published toxicity thresholds for the individual contaminants present in the firefighting wastewater. While individual thresholds do not account for mixture synergism, comparing measured concentrations against species-specific effect concentrations (EC_{50}, NOEC, LOEC) reported in the literature remains essential to identify the primary chemical drivers navigating the effluent's overall toxicity.

The experimental results for barrel A and B reveal an extreme level of aquatic toxicity that aligns with, and in some cases exceeds, established toxicological literature for LIB effluents. For *Daphnia magna*, the observed EC_{50} values (reaching as low as 0.05 % of the raw sample) are consistent with the known high sensitivity of crustaceans to lithium (LC50 ≈16 mg/L according to Hamilton (1995)) and the synergistic effect of fluorides (F^-), which typically become acutely toxic at concentrations above 100 mg/L (Camargo, 2003). In contrast, the lower sensitivity of *Aliivibrio fischeri* (where EC_{50} values were only reached at high wastewater percentages) reflects the higher bacterial tolerance to lithium-ion concentrations, which typically require thresholds exceeding 2,755 mg/L for significant bioluminescence inhibition (Roh and Sung, 2023). The phytotoxicity observed in *Lemna minor* (growth inhibition $EC_{50} \approx 1.4$ %) corresponds with lithium's ability to interfere with plant ion transport and photosynthetic efficiency at levels above 30 mg/L (Kszos and Stewart, 2003). Furthermore, the severe dehydrogenase activity (DHA) inhibition in soils (up to 80 %) highlights a profound disruption of microbial respiration, likely driven by the bioavailability of lithium and fluoride ions in the acidic Lufa 2.2 environment (Wolińska and Stępniewska, 2012). Collectively, these data confirm that the measured concentrations of lithium (up to 1.5 g/L) and fluorides (up to 190 mg/L) create a highly hazardous effluent that undergoes significant toxicological maturation, necessitating robust treatment before environmental discharge.

In contrast to the extreme toxicity observed in the other samples, barrel C exhibited a significantly different toxicological profile, characterized by lower initial toxicity and a more gradual increase in hazardous potential. For *Daphnia magna*, the initial EC_{50} (48 h) of 16.32 % suggests a much lower concentration of bioavailable pollutants compared to barrel B, likely due to a higher water-to-battery ratio or a different battery chemistry. However, a notable "maturation" of the waste was observed, as toxicity intensified nearly tenfold by day 112 ($EC_{50} \approx 1.8$ %). Interestingly, barrel C demonstrated the highest sensitivity in the *Aliivibrio fischeri* test (EC_{50} at approximately 1.8 % by day 112), which is atypical for lithium alone and suggests a specific accumulation of organic electrolyte degradation products or other soluble inhibitors. This extreme microbial toxicity may be primarily driven by the unique diversity of oxygenated heterocyclic compounds (such as 2-methylfuran, 2,5-dimethylfuran, and 2-acetyl-5-methylfuran) and unreacted volatile organics detected via GC-MS. Because barrel C did not undergo open combustion, these highly toxic organic electrolyte degradation products were preserved and slowly leached into the aqueous phase rather than being destroyed by flames, indicating that non-ignited venting events present an equal, if distinct, hazard to aquatic microbiomes. Regarding soil health, barrel C showed minimal impact on DHA (dehydrogenase activity), with results fluctuating near the baseline (ranging from minor stimulation to 21.4 % inhibition). This indicates that while the aquatic ecosystem remains at risk from barrel C effluent, the soil microbial respiration was significantly less compromised than in the presence of the more concentrated lithium and fluoride levels found in barrels A and B.

4.4. Regulatory compliance and pre-treatment necessity

The extreme concentrations of contaminants observed in this study, particularly in cases of severe battery destruction (barrel B), present a significant challenge for compliance with existing and emerging European water legislation. While the Drinking Water Directive (EU) 2020/2184 mandates a strict fluoride limit of 1.5 mg/L to protect human health, industrial and urban wastewater discharge is typically governed by localized sewer use regulations, which often set fluoride limits between 15 and 30 mg/L to prevent the corrosion of concrete infrastructure. Our results showed fluoride levels reaching up to 218.2 mg/L, exceeding these typical sewer discharge limits by nearly tenfold. Furthermore, while lithium currently lacks a universal EU-wide discharge limit, its inclusion in the 2026 Watch List under the Water Framework Directive highlights its status as a pollutant of emerging concern. The lithium concentrations measured in this study (peaking at 1.5 g/L) are several orders of magnitude higher than any anticipated ecological or municipal threshold.

In current practice, emergency units in several European countries already deploy mobile containment systems for hazardous firefighting runoff – such as portable retention basins, heavy-duty bladders, inflatable berms, or sealed fire-water traps – to prevent uncontrolled discharge into stormwater drains (EPA, 2019; SEPA et al., 2000; VdS Schadenverhütung GmbH, 2004). These systems are analogous to those used for industrial fires, chemical spills, and contaminated road runoff, where the priority is immediate hydraulic containment rather than treatment. However, during an active vehicle fire, emergency units prioritize life safety and immediate fire suppression, making the active containment of high-flow runoff on an open roadway operationally unfeasible in the moment.

Managing this unique effluent requires specialized mobile or stationary on-site containment systems, such as temporary heavy-duty retention bladders or specialized fire suppression water-traps deployed by emergency units. Traditional municipal wastewater facilities or road runoff oil-water separators are entirely unequipped to manage the dissolved lithium and fluoride loads identified in this study. Effective treatment must leverage a two-stage physico-chemical process: initial pH neutralization combined with calcium chloride ($CaCl_2$) or lime ($Ca(OH)_2$) dosing to induce the precipitation of insoluble calcium fluoride (CaF_2), followed by advanced ion exchange or specialized precipitation matrices (such as sodium carbonate at elevated temperatures) to capture the highly mobile lithium ions.

5. Conclusions

This study demonstrates that the environmental impact of lithium-ion battery (LIB) fire suppression is a critical, yet overlooked, drawback of electromobility. Our 112-day immersion experiment reveals that the severity of battery destruction directly dictates the pollutant load, with fully compromised modules generating wastewater with conductivity levels (23.1 mS/cm) comparable to landfill leachates.

Key findings indicate that lithium and fluoride concentrations can reach 1.54 g/L and 218.2 mg/L, respectively, exceeding typical regulatory discharge limits by several orders of magnitude. Furthermore, a significant temporal "maturation" of toxicity was observed; EC_{50} values for *Daphnia magna* reached as low as 0.05 % after extended submersion, indicating that the ecological hazard intensifies over time as bioavailable contaminants leach from the cells. Notably, even non-ignited modules that only vent electrolyte smoke release hazardous organic pollutants and exhibit high microbial toxicity, as demonstrated by an acute *Aliivibrio fischeri* EC_{50} value of 1.8 %.

Ultimately, these results underscore that standard urban wastewater treatment is insufficient for managing such concentrated streams. To prevent the breakthrough of toxic elements like lithium and fluoride into aquatic ecosystems, specialized on-site containment and pre-treatment protocols must be integrated into emergency response strategies for electric vehicle incidents.

CRediT authorship contribution statement

Lucie Pokorna-Krayzelova: Conceptualization, Data curation, Investigation, Methodology, Project administration, Writing – original draft. **Hana Kujalova:** Data curation, Investigation, Writing – review & editing. **Lucia Tajnaiova:** Data curation. **Klara Anna Mocova:** Data curation. **Martina Martinková:** Data curation. **Jana Kofronová:** Data curation. **Radek Vurm:** Data curation. **Jakub Pilar:** Data curation. **Krystof Rehak:** Data curation. **Barbora Stepanova:** Writing – review & editing. **Petra Najmanova:** Writing – review & editing. **Jan Karl:** Writing – review & editing. **Romana Friedrichova:** Data curation. **Marek Martinec:** Data curation, Methodology. **Jan Bindzar:** Conceptualization, Data curation, Investigation, Methodology, Writing – review & editing.

Declaration of competing interest

The authors declare that they have no known competing financial interests or personal relationships that could have appeared to influence the work reported in this paper.

Acknowledgements

This contribution was created with the special support of Ministry of the Interior, Czech Republic from the project VB02000068 "FiLiB - Protection of the population and emergency response units against emissions from fire of Li-Ion batteries" within the framework of the Czech Republic Security Research Program, development, testing and evaluation of new security technologies (SECTECH).

Supplementary materials

Supplementary material associated with this article can be found, in the online version, at doi:10.1016/j.watres.2026.126751.

Data availability

Data will be made available on request.

References

Aaltonen, M., Peng, C., Wilson, B.P., Lundström, M., 2017. Leaching of Metals from Spent Lithium-Ion Batteries, p. 20.
Alum, B.N., Echegu, D.A., Alum, E.U., Uti, D.E., Egba, S.I., Aleke, J.U., 2026. Lithium-ion batteries as a cornerstone of electric vehicle advancement: innovations, challenges, and policy implications. Top. Curr. Chem. 384 (2), 14.
APHA, 2012. Standard Methods for the Examination of Water & Wastewater. American Public Health Association (APHA), American Water Works Association (AWWA) & Water Environment Federation (WEF), Washington D.C.
Benaddi, R., Ferkan, Y., Bouriqi, A., Ouazzani, N., 2022. Impact of landfill leachate on groundwater quality–a comparison between three different landfills in Morocco. J. Ecol. Eng. 23 (11), 89–94.
Bisschop, R., Willstrand, O., Rosengren, M., 2020. Handling lithium-ion batteries in electric vehicles: preventing and recovering from hazardous events. Fire Technol. 56 (6), 2671–2694.
Camargo, J.A., 2003. Fluoride toxicity to aquatic organisms: a review. Chemosphere 50 (3), 251–264.
Cui, Y., Liu, J., Han, X., Sun, S., Cong, B., 2022. Full-scale experimental study on suppressing lithium-ion battery pack fires from electric vehicles. Fire Saf. J. 129, 103562.
EPA, 2019. Environmental Protection Agency Guidance on Retention Requirements for Firewater Run-off. Environmental Protection Agency.
Geldasa, F.T., Kebede, M.A., Shura, M.W., Hone, F.G., 2022. Identifying surface degradation, mechanical failure, and thermal instability phenomena of high energy density Ni-rich NCM cathode materials for lithium-ion batteries: a review. RSC Adv. 12 (10), 5891–5909.
Gouveia, J.R., Ribeiro, I., Oliveira, L., Lourenço, E., Neto, B., 2026. The future of sustainable lithium-ion batteries: ecodesign recommendations for solid-state technologies. Energy Storage Mater. 90, 105312.
Hamilton, S.J., 1995. Hazard assessment of inorganics to three endangered fish in the Green river, Utah. Ecotoxicol. Environ. Saf. 30 (2), 134–142.
Hammed, V.O., Salako, E.W., Edet, D., Ederhion, J., Keshinro, B.I., Uwaoma, I.A., Adeleke, O.J., Odetoran, A., Adedokun, O.J., Makinde, P.F., Alli, Y.A., 2025. Next-generation lithium-ion batteries for electric vehicles: advanced materials, AI driven performance optimization, and circular economy strategies. Meas.: Energy 7, 100060.
Hoban, C., Parkinson, N., Jayanthi, K., Paranthaman, M.P., Navrotsky, A., Woodfield, B. F., 2025. Impact of anions and water content on [Li–Al] layered double-hydroxide stability. J. Phys. Chem. C 129 (1), 793–800.
Hynynen, J., Willstrand, O., Blomqvist, P., Andersson, P., 2023. Analysis of combustion gases from large-scale electric vehicle fire tests. Fire Saf. J. 139, 103829.
IEA, 2024. Global EV Outlook 2024: Moving Towards INCREASED affordability. Agency, I.E., Paris.
IEA, 2025. Global EV Outlook 2025. Agency, I.E., Paris.
Jalali, H., Collie, L., Baroutian, S., 2026. Air emissions & firewater runoff contamination from lithium-ion battery fires in rubbish trucks. Environ. Pollut. 389, 127437.
Jiaqiang, E., Xiao, H., Tian, S., Huang, Y., 2024. A comprehensive review on thermal runaway model of a lithium-ion battery: mechanism, thermal, mechanical, propagation, gas venting and combustion. Renew. Energy 229, 120762.
Krupińska, I., 2020. Aluminium drinking water treatment residuals and their toxic impact on human health. Molecules 25 (3), 641.
Kszos, L.A., Stewart, A.J., 2003. Review of lithium in the aquatic environment: distribution in the United States, toxicity and case example of groundwater contamination. Ecotoxicology 12 (5), 439–447.
Kulkarni, S., Duan, K., Pang, G., Bhatti, A., 2026. Recent advancements and perspectives in lithium-ion battery technology. Energy Strategy Rev. 64, 102064.
Lai, X., Yao, J., Jin, C., Feng, X., Wang, H., Xu, C. and Zheng, Y. 2022 A review of lithium-ion battery failure hazards: test standards, accident analysis, and safety suggestions, p. 248.
Larsson, F., Andersson, P., Blomqvist, P., Lorén, A., Mellander, B.E., 2014. Characteristics of lithium-ion batteries during fire tests. J. Power Sources 271, 414–420.
Larsson, F., Andersson, P., Blomqvist, P., Mellander, B.E., 2017. Toxic fluoride gas emissions from lithium-ion battery fires. Sci. Rep. 7.
Lazarenko, O.V., Synelnikov, O.D., Bykov, I.M., Kuskovets, A.S., 2019. Fire extinguishing and other urgent work in electric cars. Fire Saf. 54–58.
Lecocq, A., Bertana, M., Truchot, B., Marlair, G., 2012. Comparison of the Fire Consequences of an Electric Vehicle and an Internal Combustion Engine Vehicle. SP Technical Research Institute of Sweden, Boras, Chicago, United States, pp. 183–194.
Li, H., Peng, W., Yang, X., Chen, H., Sun, J., Wang, Q., 2020. Full-scale experimental study on the combustion behavior of lithium ion battery pack used for electric vehicle. Fire Technol. 56 (6), 2545–2564.
Lu, L.G., Han, X.B., Li, J.Q., Hua, J.F., Ouyang, M.G., 2013. A review on the key issues for lithium-ion battery management in electric vehicles. J. Power Sources 226, 272–288.
Mao, Y., Chen, Y., Chen, M., 2024. Review of flame behavior and its suppression during thermal runaway in lithium-ion batteries. Batteries 10 (9), 307.
Meraner, C., Fjærestad, J.S., Vullum-Bruer, F., Stefanska, M., Li, T., 2026. Suppression of battery energy storage system fires. Fire Saf. J. 162, 104727.
Mukhamed'yarova, A.N., Gareev, B.I., Nurgaliev, D.K., Aliev, F.A. and Vakhin, A.V. 2021 A review on the role of amorphous aluminum compounds in catalysis: avenues of investigation and potential application in petrochemistry and oil refining, p. 1811.
Muratori, M., Alexander, M., Arent, D., Bazilian, M., Cazzola, P., Dede, E.M., Farrell, J., Gearhart, C., Greene, D., Jenn, A., Keyser, M., Lipman, T., Narumanchi, S., Pesaran, A., Sioshansi, R., Suomalainen, E., Tal, G., Walkowicz, K., Ward, J., 2021. The rise of electric vehicles-2020 status and future expectations. Prog. Energy 3 (2).

Nitta, N., Wu, F., Lee, J.T., Yushin, G., 2015. Li-ion battery materials: present and future. Mater. Today 18 (5), 252–264.
Ping, P., Wang, Q., Huang, P., Li, K., Sun, J., Kong, D., Chen, C., 2015. Study of the fire behavior of high-energy lithium-ion batteries with full-scale burning test. J. Power Sources 285, 80–89.
Pražanová, A., Kočí, J., Míka, M.H., Pilnaj, D., Plachý, Z., Knap, V., 2023. Pre-recycling material analysis of NMC lithium-ion battery cells from electric vehicles. Crystals 13 (2), 214.
Quant, M., Willstrand, O., Mallin, T., Hynynen, J., 2023. Ecotoxicity evaluation of fire-extinguishing water from large-scale battery and battery electric vehicle fire tests. Environ. Sci. Technol. 57 (12), 4821–4830.
Rensmo, A., 2022. In: Per- and Polyfluoroalkyl Substance (PFAS) Emissions from Recycling Processes of Lithium-Ion Batteries, PhD thesis. UPTEC K, 22017.
Roh, I., Sung, K., 2023. Ecotoxicity of *Daphnia magna* and *Aliivibrio fischeri* on potentially harmful substances emissionsfrom battery manufacturing processes: lithium, nickel, and sulfate. J. Environ. Impact Assess. 32 (2), 123–133.
Sanguesa, J.A., Torres-Sanz, V., Garrido, P., Martinez, F.J., Marquez-Barja, J.M., 2021. A review on electric vehicles: technologies and challenges. Smart Cities-Basel 4 (1), 372–404.
SEPA, Scottish Environment Protection Agency, Environment Agency and Environment and Heritage Service, 2000. Managing Fire Water and Major Spillages: Pollution Prevention Guidelines (PPG18). Environment Agency, Bristol, United Kingdom.
Shahid, S., Agelin-Chaab, M., 2022. A review of thermal runaway prevention and mitigation strategies for lithium-ion batteries. Energy Convers. Manag. 16, 100310.
Shen, R., Quan, Y., McIntosh, J.D., Salem, A., Wang, Q., 2024. Fire safety of battery electric vehicles: hazard identification, detection, and mitigation. SAE Int. J. Electrified Veh. 13 (3), 279–294.
Sturm, P., Fößleitner, P., Fruhwirt, D., Galler, R., Wenighofer, R., Heindl, S.F., Krausbar, S., Heger, O., 2022. Fire tests with lithium-ion battery electric vehicles in road tunnels. Fire Saf. J. 134, 103695.
Sun, P., Bisschop, R., Niu, H., Huang, X., 2020. A review of battery fires in electric vehicles. Fire Technol. 56 (4), 1361–1410.
VdS Schadenverhütung GmbH, 2004. DS-Richtlinien für Löschwasser-Rückhalteanlagen - Bauteile und Systeme - Anforderungen und Prüfmethoden - Teil 1: Stationäre Löschwasserbarrieren. VdS Schadenverhütung GmbH, Köln, Germany.
Wang, Q.S., Ping, P., Zhao, X.J., Chu, G.Q., Sun, J.H., Chen, C.H., 2012. Thermal runaway caused fire and explosion of lithium ion battery. J. Power Sources 208, 210–224.
Watanabe, I., Sakai, S.-I., 2003. Environmental release and behavior of brominated flame retardants. Environ. Int. 29 (6), 665–682.
Wellburn, A.R., 1994. The spectral determination of chlorophylls a and b, as well as total carotenoids, using various solvents with spectrophotometers of different resolution. J. Plant Physiol. 144 (3), 307–313.
Wolińska, A., Stępniewska, Z., 2012. Dehydrogenase activity in the soil environment. Dehydrogenases 10, 183–210.
Xu, K., 2014. Electrolytes and interphases in Li-ion batteries and beyond. Chem. Rev. 114 (23), 11503–11618.
Zaino, R., Ahmed, V., Alhammadi, A.M., Alghoush, M., 2024. Electric vehicle adoption: a comprehensive systematic review of technological. Environmental, Organizational and Policy Impacts, p. 375.
Zhang, Y., Wang, H., Li, W., Li, C., 2019. Quantitative identification of emissions from abused prismatic Ni-rich lithium-ion batteries. ETransportation 2, 100031.